Available online at www.sciencedirect.com
ScienceDirect
Optics & Laser Technology 39 (2007) 549–557
Optics & Laser Technology
www.elsevier.com/locate/optlastec

Research on the processing experiments of laser metal deposition shaping

Kai Zhang[a,b,*], Weijun Liu[a], Xiaofeng Shang[a,c]

[a]*Shenyang Institute of Automation, Chinese Academy of Sciences, Shenyang 110016, China*
[b]*Graduate School of the Chinese Academy of Sciences, Beijing 100049, China*
[c]*Shenyang Institute of Aeronautical Engineering, Shenyang 110034, China*

Received 22 July 2005; received in revised form 27 October 2005; accepted 28 October 2005
Available online 6 December 2005

Abstract

Laser additive direct deposition of metals is a new rapid manufacturing technology, which combines with computer-aided design (CAD), laser cladding and rapid prototyping. The advanced technology can build fully dense metal components directly from CAD files with neither mould nor tool. Based on the theory of this technology, a promising rapid manufacturing system called ''Laser Metal Deposition Shaping (LMDS)'' has been constructed and developed successfully by Chinese Academy of Sciences, Shenyang Institute of Automation. Through the LMDS system, comprehensive experiments are carried out with nickel-based superalloy to systematically investigate the influences of the processing parameters on forming characteristics. By adjusting to the optimal processing parameters, fully dense and near-net-shaped metallic parts can be directly obtained through melting coaxially fed powder with a laser. Moreover, the microstructure and mechanical properties of as-formed samples are tested and analyzed synthetically. As a result, significant processing flexibility with the LMDS system over conventional processing capabilities is recognized, with potentially lower production cost, higher quality components, and shorter lead-time.

Keywords: Laser metal deposition shaping (LMDS); Nickel-based superalloy components; Processing parameters; Forming characteristics; Microstructure and property

1. Introduction

Laser additive direct metal deposition refers to the additive-layered manufacturing technology for building components from a computer-aided design (CAD) model without the use of forming dies, tooling or machining [1,2]. The principle of this technology is based on the selective laser sintering (SLS) and laser cladding. A motion control program, developed from the CAD model of a desired metal component, is used to control the motion of a laser focal spot to trace all areas of the component on a substrate, typically a planar layer at a time. Metal powder particles, injected into the laser focal zone, are melted and then re-solidify into the prior-deposited fully dense metal part in the wake of the moving molten pool created by the laser beam. Simultaneously, the substrate is moved in the X–Y plane (see Fig. 1) beneath the laser beam to deposit a thin cross-section, thereby creating the desired geometry for each layer. After deposition of each layer, the powder delivery nozzle and focusing lens assembly is incremented in the positive Z-direction (see Fig. 1) [3]. As a result, successive layers are then stacked to produce the entire component volume of fused metal representing the desired CAD model [4,5], thereby building a three-dimensional component additively. In nature, this forming procedure is multi-layer laser cladding.

With the ability of one-step manufacture, the technology can greatly reduce the lead-time and investment cost of module and die design, the fabrication of hard or rare metal components, the repair of refractory and costly components, etc [6]. With this technology, there is no

*Corresponding author. Shenyang Institute of Automation, Chinese Academy of Sciences, Shenyang 110016, China. Tel.: +86 24 2397 0297; fax: +86 24 2397 0534.
E-mail address: kzhang@sia.cn (K. Zhang).

0030-3992/$ - see front matter © 2005 Elsevier Ltd. All rights reserved.
doi:10.1016/j.optlastec.2005.10.009

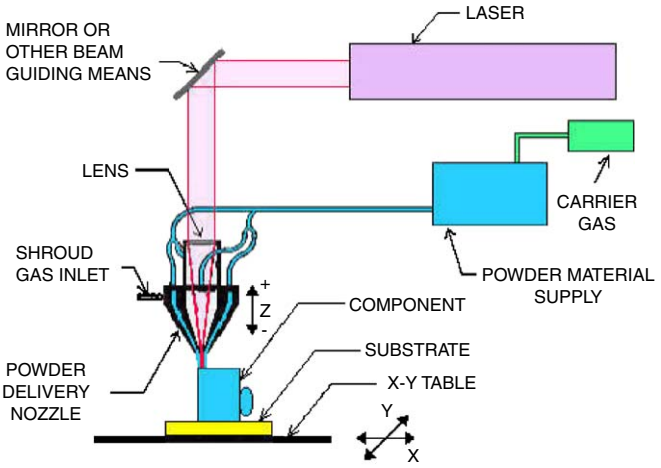

Fig. 1. The diagrammatic sketch of the LMDS system.

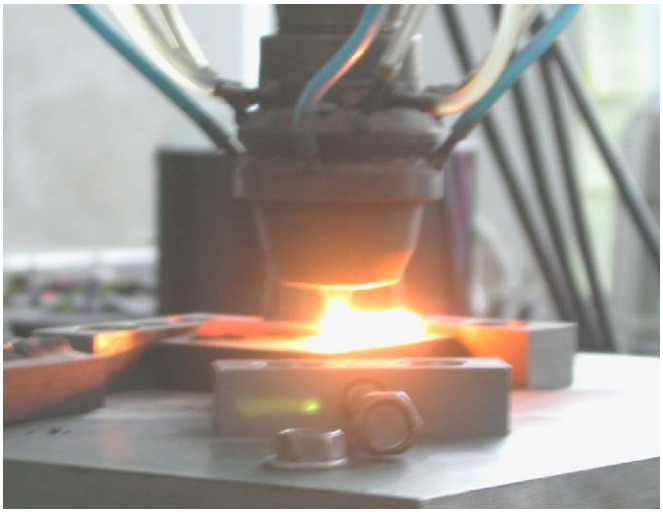

Fig. 2. The working coaxial powder nozzle of the LMDS system.

interference between tools and formed parts, so the geometrical shape can be very complicated [7]. Moreover, the as-deposited parts are fully dense, hold rapid-solidified microstructure, and meet the requirements for direct usage. The technology shows extensive application on many fields, such as aerospace, planes, and weapons [8]. By virtue of such conspicuous and attractive advantages, development of this technology has been pursued at many scientific research academies and universities all over the world, which results in some similar fabrication processes. Recently, a promising rapid manufacturing system called "Laser Metal Deposition Shaping (LMDS)" has been constructed and developed with flying colors by Chinese Academy of Sciences, Shenyang Institute of Automation. Depending on this manufacturing system, substantive experiments are carried out to investigate the effects of different processing parameters on the forming characteristics. Based on these research results, some functionally metallic components are fabricated successfully. The present work describes our researches on this subject.

2. Experimental condition and procedure

2.1. Experimental condition

The experiments are carried out with the LMDS system, which consists of a 2 kW continuous wave CO_2 laser, a precisely three-dimensional numerical control working table and a powder feeder with coaxial nozzle (see Fig. 2). The powder used in the experiments is nickel-based superalloy, whose composition is listed in Table 1. The substrate used for multi-layer laser cladding is A3 steel plate with the dimension of $60 \times 60 \times 10\,mm^3$.

2.2. Experimental procedure

In order to investigate the influences of processing parameters on forming characteristics, single-cladding pass with the length of 50 mm is continuously clad for 10 layers on substrate corresponding to the diverse processing parameters, which are listed in Table 2. Argon is used as shielding gas to protect the molten pool from oxidizing. In order to ensure the cladding condition of each layer is identical, the focusing mirror and the nozzle are matched together. After each layer is finished, they lift a little distance, which is equal to the height of single layer. The dimension of each specimen is measured with a spiral micrometer and compared with each other so as to investigate the forming characteristics under different processing parameters, for example, the height of single-cladding layer and the width of single-cladding pass [9]. By comparing the forming quality of each set of processing parameters, the suitable parameters can be selected to conduct the planar scanning experiments, so the most appropriate scanning space is confirmed. Based on these optimal parameters, a series of experiments are carried out to get some functionally metallic parts. Moreover, SEM is used to analyze the microstructure of cladding layers, energy spectrometer is applied to test the composition segregation of alloy elements, and microhardness instrument is utilized to measure the hardness distribution of

Table 1
The chemical composition of the powder (wt.%)

Powder	C	Al	Si	Cr	Fe	Ni
Nickel-based superalloy	0.5	0.3	0.45	19	1.4	Bal

Table 2
The list of processing parameters

Laser power (W)	Scanning velocity (mm/s)	Spot diameter (mm)	Powder feeding rate (g/min)
500–900	2–10	2–4	2–10

cladding layers. Additionally, standard tensile sample is fabricated by the LMDS system to test mechanical properties, and the fracture appearance of the tensile sample is observed through the SEM.

3. Results and analysis

3.1. The effects of processing parameters on forming characteristics

The forming characteristics are mainly affected by the processing parameters, so the optimal processing parameters are the key to get excellent forming parts. Investigating the influencing regularity of processing parameters on forming characteristics is the significant method to obtain the optimal processing parameters.

3.1.1. The height of single-cladding layer

The height of single-cladding layer is a very important forming characteristic concerning the LMDS technology. Not only does it determine the fabrication efficiency, but also controls the fabrication precision of vertical direction. At the present research level, vertical fabrication precision relative to horizontal one is so low as to affect the whole accuracy of the as-fabricated parts. Accordingly, investigating the relationship between different processing parameters and the height of single-cladding layer is comparatively significant.

3.1.1.1. The effects of powder-feeding rate and scanning velocity. Since powder-feeding rate and scanning velocity obviously determine the quantity of powder sprayed into molten pool and the intensity of the laser energy absorbed by substrate and powder in unit time, to a great extent, they dominate the height of single-cladding layer. Consequently, they must be restricted in a certain range so as to make the height of single-cladding layer formed by the fused metallic powder matching the thickness of sliced CAD model. Otherwise, the accumulative multi-layer errors in height direction can lead to the collapse with forming parts [10,11].

Fig. 3 shows the influences of powder-feeding rate Q (g/min) and scanning velocity V (mm/s) on the height of single-cladding layer H (mm). Seeing from it, on condition that laser power P (W) and spot diameter D (mm) keep constant, affected by the quantity of powder sprayed into the molten pool in unit time, the height of single-cladding layer ascends accompanying the augment of powder-feeding rate and descends with the increase of scanning velocity. When powder-feeding rate is 10 g/min and scanning velocity is faster than 6 mm/s, the incontinuous scanning beam appears. The reason why this case happens is that the laser irradiation energy is not enough to entirely melt material and form stable molten pool.

3.1.1.2. The effects of laser power and spot diameter. The effects of laser power and spot diameter on the height of single-cladding layer are relatively intricate in that they interact with each other intimately. In order to synthetically consider the effects, a significant parameter, laser power density, namely the ratio of laser power to spot area, is induced to develop the research. The greatly low laser power density leads a series of defects, such as powder adherence, aperture, and low bonding intensity, even the incontinuous scanning beam. Contrarily, the extremely high laser power density easily causes the over-sintering of the powder and the oxidation of the microstructure. Consequently, it is important to control the laser power density in a certain suitable scope.

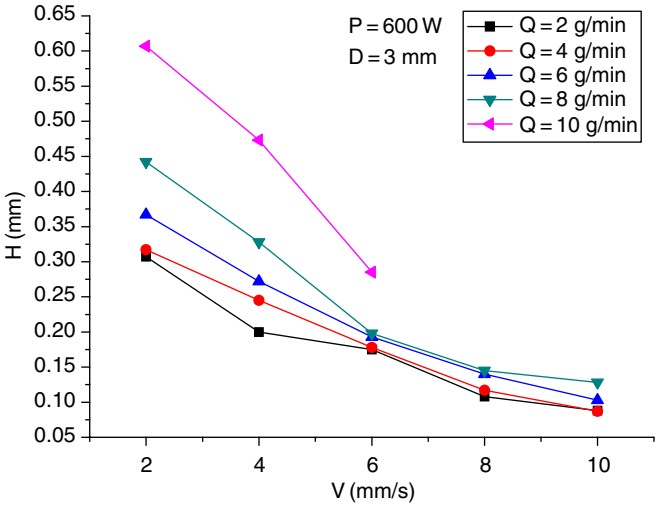

Fig. 3. The influences of powder-feeding rate and scanning velocity on the height of single-cladding layer.

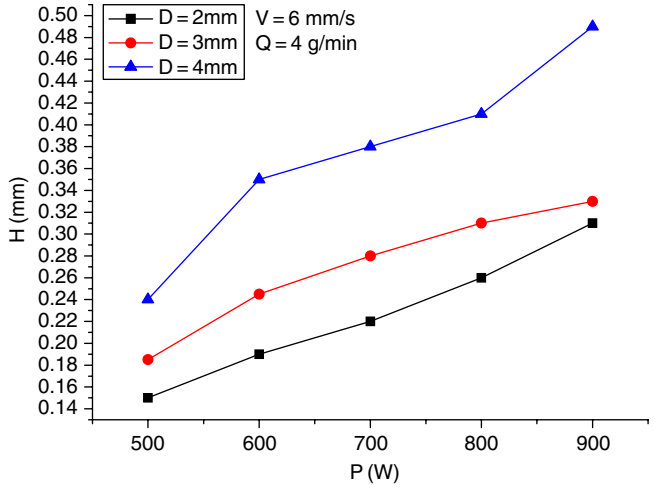

Fig. 4. The influences of laser power and spot diameter on the height of single-cladding layer.

Fig. 4 demonstrates the influences of laser power P (W) and spot diameter D (mm) on the height of single-cladding layer H (mm). The regularity can be found from it: With the increase of laser power and spot diameter, the height of single-cladding layer goes up on condition that scanning

velocity V (mm/s) and powder-feeding rate Q (g/min) hold invariant.

3.1.2. The width of single-cladding pass

The width of single-cladding pass is another significant factor in terms of LMDS technology. It is mainly restricted by the dimension of molten pool, and has a strong affinity for laser power, spot diameter, scanning velocity and powder-feeding rate.

3.1.2.1. The effects of powder-feeding rate and scanning velocity. Fig. 5 exhibits that if laser power P (W) and spot diameter D (mm) hold immutable, the width of single-cladding pass W (mm) increases accompanying the rise of powder-feeding rate Q (g/min), but decreases with the augment of scanning velocity V (mm/s). As powder-feeding rate is 10 g/min and scanning velocity is faster than 6 mm/s, the laser irradiation energy absorbed by the powder and substrate is too deficient to fully melt them and reach metallurgic bonding. Accordingly, the advent of discontinuous scanning beam gives birth to the interruption of forming process.

3.1.2.2. The effects of laser power and spot diameter. The influencing regularity of laser power P (W) and spot diameter D (mm) on the width of single-cladding pass W (mm) is revealed in Fig. 6. Under the circumstances that scanning velocity V (mm/s) and powder-feeding rate Q (g/min) keep invariable, the width of single-cladding pass goes up with the increase of laser power, whereas the influence of spot diameter on the width of single-cladding pass is relatively complex: on the one hand, the big spot diameter enlarges the laser irradiation area, which is beneficial to form large molten pool and increase the width of single-cladding pass; on the other hand, the big spot diameter induces the low laser power density. As a result, the laser power density at the edge of cladding pass

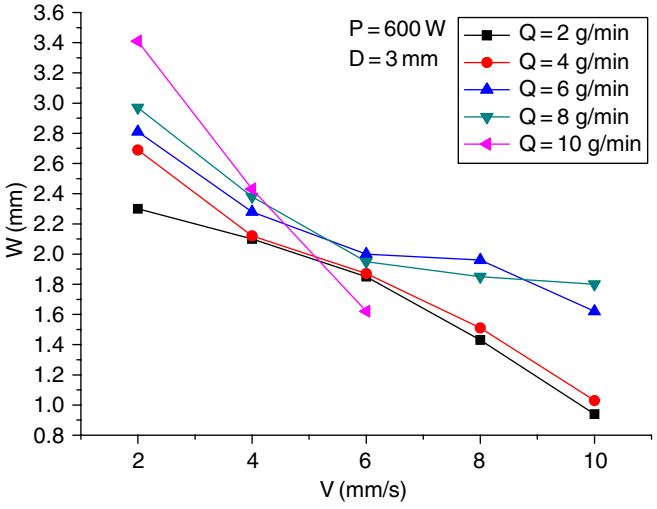

Fig. 5. The influences of powder-feeding rate and scanning velocity on the width of single-cladding pass.

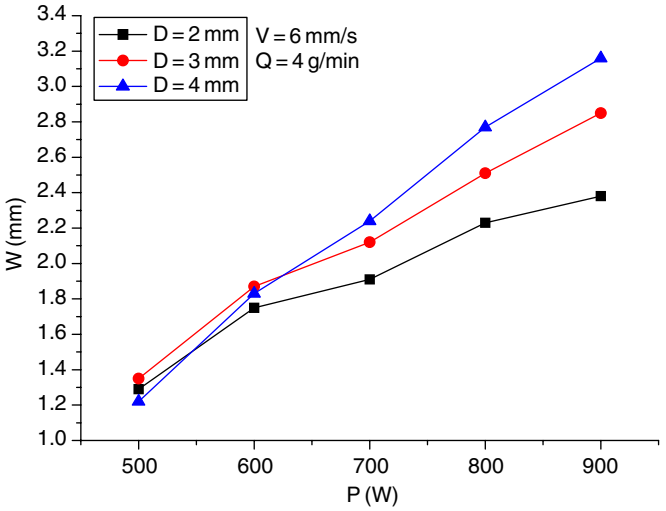

Fig. 6. The influences of laser power and spot diameter on the width of single-cladding pass.

is too weak to melt the powder and substrate, which causes that the size of molten pool and the width of single-cladding pass both decrease. Furthermore, the effect of spot diameter on the width of single-cladding pass associates with laser power and scanning velocity, which leads the influencing regularity becoming more complicated.

3.1.3. The smoothness of forming surface

Scanning space, namely overlapping rate, plays a significant role in the process of LMDS technology, which directly affects the smoothness of forming surface. During the forming process, choosing the appropriate scanning space is the key to obtain the uniform height of contiguous cladding passes, even the flat surface of as-deposited components. The exceedingly small scanning space leads to the concave at the interval of adjacent cladding passes, whereas the extremely big one causes that the latter cladding pass accumulates on the former.

Fig. 7 describes the cross section in the ideal overlapping state with two adjacent cladding passes. In this ideal overlapping state, the cladding layers hold smooth surface and full density, and the current overlapping rate is called critical overlapping rate η_c, so it is substantially important to confirm η_c. Above all, several hypotheses need to be established.

(1) The quantity of powder at each cladding pass is identical. Namely, the cross section area of each cladding pass is uniform.
(2) As can be seen from Fig. 7, the cross section of the former cladding pass is arc-shaped, and the centre of the circle is point O; the centre of the circle of the latter cladding pass is point O′, and the shape of the right section of the latter is the same as the former, whereas the cladding surface from the point O to the point O′ is smooth.
(3) The height of zenith at each cladding pass is equal.

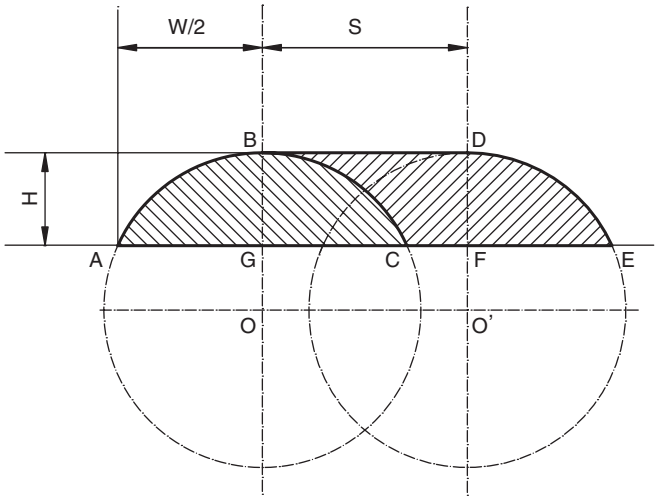

Fig. 7. The schematic diagram of the cross section in the ideal overlapping state.

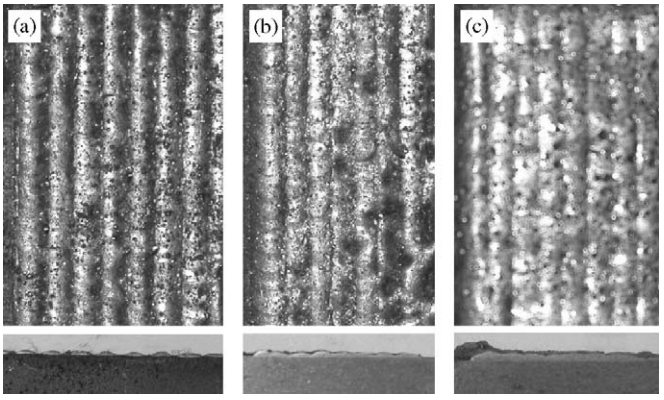

Fig. 8. Appearances of planar scanning experimental specimens. (a) Scanning space 2.1 mm. (b) Scanning space 1.7 mm. (c) Scanning space 1.3 mm.

According to hypothesis (1), the following equations can be inferred:

$$A_{ABC} = A_{BDEC} = A_{BDFG} = HS, \tag{1}$$

where A_{ABC}, A_{BDEC}, A_{BDFG} is the area of specific region, H the height of single-cladding layer, and S the ideal scanning space.

$$A_{ABC} = \left(\frac{(W/2)^2 + H^2}{2H}\right)^2 \arcsin\frac{2(W/2)H}{(W/2)^2 + H^2} - (W/2)\frac{(W/2)^2 - H^2}{2H}, \tag{2}$$

where W is the width of single-cladding pass.

From Eqs. (1) and (2), the ideal scanning space S can be represented as

$$S = \frac{((W/2)^2 + H^2/2H)^2 \arcsin 2((W/2)H)/((W/2)^2 + H^2) - (W/2)((W/2)^2 - H^2)/2H}{H}. \tag{3}$$

Accordingly, the critical overlapping rate η_c can be defined as

$$\eta_c = \frac{W - S}{W}. \tag{4}$$

In this way, based on the height of single-cladding layer H and the width of single-cladding pass W, which are measured under certain special processing parameters, the ideal scanning space S can be figured out according to Eq. (3). Consequently, the critical overlapping rate η_c can be worked out in response to Eq. (4).

Noticeably, the equations mentioned above are inferred in the ideal state. In fact, due to the action of surface tension, the overlapping surface is impossibly the absolute plane, which induces the convex arc shape with the cross section of the cladding pass and the depression between the consecutive cladding passes. Especially, the higher the cladding layer, the bigger the curvature of the cross section, so it is critical to avoid the excessively high cladding layer.

During the analysis mentioned above, a restrictive condition, namely $H \leqslant W/2$, needs to be met, which means that the cross section of the cladding pass is a semicircle at the most. Actually, in order to avoid the appearance of apertures between the contiguous cladding passes, the cladding height H should not be too great. Commonly, the critical cladding height H_c must meet the following equation:

$$H_c < \frac{2}{3} r_l, \tag{5}$$

where r_l is the laser spot radius.

After conducting planar scanning experiments with different scanning spaces, the optimal overlapping rate can be gained by observing the appearances of scanning plane. Judging from the experiments of single cladding layer and pass mentioned above, the optimal processing parameters capable of obtaining excellent forming characteristics are: laser power 700 W, spot diameter 3 mm, scanning velocity 6 mm/s, powder feeding rate 4 g/min. Under such circumstances, the height of single cladding layer H is 0.28 mm and the width of single-cladding pass W is 1.91 mm by the measure. Accordingly, bringing the measured value of H and W into Eq. (3), the ideal scanning space S 1.3 mm can be figured out, so the critical overlapping rate η_c is 32% through Eq. (4). In order to verify the feasibility of calculating optimal scanning space by the ideal overlapping model, based on the previously determinate optimal processing parameters, the different scanning spaces are selected to conduct planar scanning experiments. Appearances of planar scanning experimental specimens are shown in Fig. 8. The scanning space in

Fig. 8a–c is orderly 2.1, 1.7 mm and experiment-determined 1.3 mm. Synthetically comparing the forming results, it is found that when scanning space is 1.3 mm, the forming specimen holds the best profiles. As can be seen from Fig. 8c, the scanning plane is relatively smooth, the height of adjacent cladding passes is generally uniform, and the channel between the adjacent cladding passes is comparatively shallow. Evidently, it is feasible to consider the ideal overlapping model as the reference to confirm the optimal scanning space and direct the forming experiments. Adopting such processing parameters, the smoothness of forming surface is strongly ensured. Sequentially, according to the bedding scanning path information obtained by the sliced CAD model, the continuous multi-layer planar scanning can be achieved successfully, which is the essence of forming whole parts.

Table 3
The optimal processing parameters

Laser power (W)	Scanning velocity (mm/s)	Spot diameter (mm)	Powder feeding rate (g/min)	Scanning space (mm)
700	6	3	4	1.3

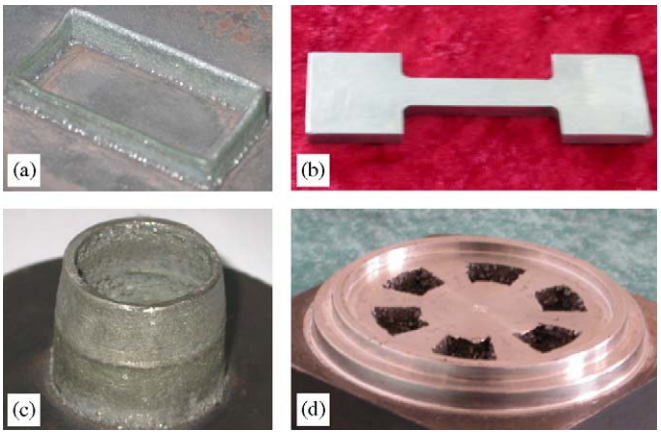

Fig. 9. Nickel-based superalloy components fabricated using LMDS system. (a) Rectangular thin-wall sample. (b) Standard tensile sample. (c) Conical tube sample. (d) Rotary table sample.

3.2. The fabrication of LMDS-fabricated parts

Based on the systematical investigation of the processing parameters, which are applied to respective experiment, a series of optimal processing parameters listed in Table 3 are selected to fabricate some nickel-based superalloy components through the LMDS system, four of which are exhibited in Fig. 9. The first part is a sample of rectangular thin-wall (see Fig. 9a); the second one is a standard tensile sample (see Fig. 9b); the third one is a sample of conical tube (see Fig. 9c); and the last one is a sample of rotary table (see Fig. 9d). All of them demonstrate fine appearances and surface quality. Besides, they are free of porosity, fully dense, and near-net shaped. Of course, they are slightly machined to obtain higher accuracy and smoothness.

3.3. The microstructure of LMDS-fabricated parts

Fig. 10a shows the SEM micrograph of the longitudinal section of the middle of cladding layer, which is fabricated with the processing parameters given in Table 3, in the Z-direction. It can be seen that the solidification microstructure is composed of parallel dendrites whose growing direction is nearly parallel to the positive Z-direction, and the dendrites take on the look of typical directional solidification microstructure in the Z-direction. In the process of cooling solidification of the liquid metal, duo to the cooling effect caused by the substrate, heat mostly dissipates in the negative Z-direction, so the temperature gradient in the positive Z-direction is remarkably dominant, which leads to the liquid metal holding the directivity. Under the action of the highest temperature gradient and solidification rate in the Z-direction, grains grow with the directional selection, thus forming the dendrites, which are almost parallel to Z-direction.

Fig. 10b displays the SEM micrograph of the longitudinal section of the top of cladding layer in the Z-direction. Apparently, equiaxed grains appear on the top of the fine dendrites.

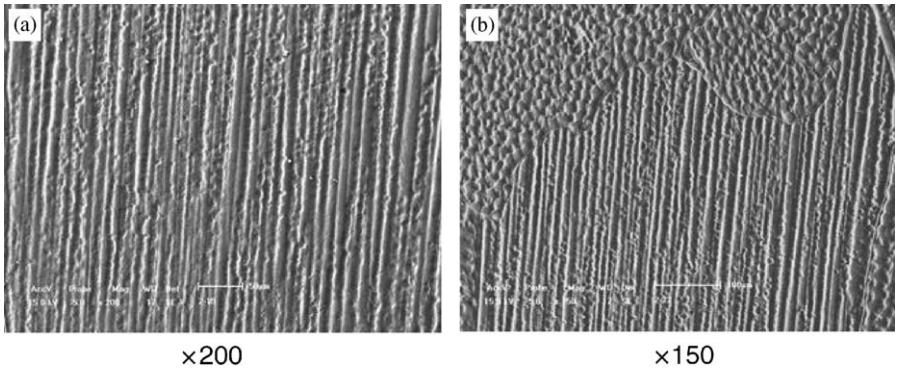

Fig. 10. SEM micrograph of the longitudinal section of LMDS-fabricated sample in the Z-direction. (a) At the middle of cladding layer. (b) At the top of cladding layer.

This phenomenon can be explained through the theory of solidification. The mechanical properties of LMDS-fabricated parts are determined by the solidification microstructure, while the solidification microstructure essentially depends on the local solidification conditions (solidification rate V_S, temperature gradient at the solid/liquid interface G), so the ratio of G to V_S, namely G/V_S, is the critical controlling parameter, which determines the feature of solidification microstructure. When the ratio of G/V_S is rather big, the solidification process prefers forming the dendritic grain structure; while the ratio of G/V_S is relatively small, the solidification process prefers forming the equiaxed grain structure. During the solidification of molten pool, as for the inside of the cladding layer, the heat dissipation and temperature gradient G are both the greatest in the Z-direction. Accordingly, the growing rate of grains in the Z-direction is faster than that in any other direction. These growing grains, which possess the directivity obstruct and even merge the grains, which grow in other directions, so the dendrites holding the feature of directional solidification are obtained eventually. However, from inside to top of the cladding layer, the temperature gradient G in the positive Z-direction gradually decreases.

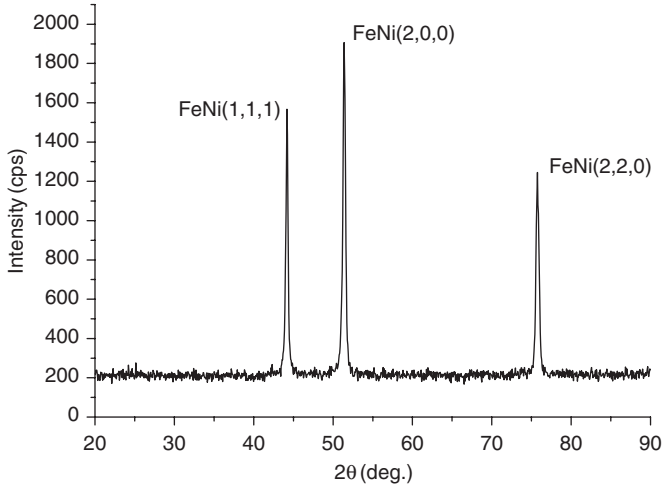

Fig. 11. The X-ray diffraction result of the surface of the nickel-based superalloy cladding layer.

At the surface of the cladding layer, the temperature gradient G in the positive Z-direction is not dominant any more. Additionally, the process that the heat dissipates from the surface is helpful to the metallic solidification, thus changing the distribution of the temperature gradient G at the top of the cladding layer. As a result, G/V_S in the Z-direction in this region decreases substantially, which causes that G/V_S in this region does not hold evident directivity any longer, thereby forming the fine-equiaxed grain structure.

Fig. 11 demonstrates the X-ray diffraction result of the surface of the nickel-based superalloy cladding layer, from which it can be found that at the surface of the cladding layer, the peak of (1 1 1), (2 0 0) and (2 2 0) crystal orientations is quite evident, which manifests that at the top of the cladding layer, the growing directions of grains are rather disorderly, and the solidification microstructure is not the directional solidification dendrite any longer.

3.4. The mechanical properties of LMDS-fabricated parts

With the LMDS-fabricated standard sheet tensile sample (see Fig. 9b), the normal temperature tensile experiment is performed along the scanning direction. As a result, the experimental data of mechanical properties are ultimate strength 430 MPa, yield strength 355 MPa and elongation percentage 9%. These data indicate that the tensile sample holds fine mechanical properties, meeting the requirement of properties for real usage.

By observing the SEM morphologies of fracture appearance of the tensile sample, which are shown in Fig. 12, a large number of dimples with various shape and size, which are distributed on the fracture can be found, and the dimples indicate that composition phases hold rather high ductility. From Fig. 12, it can be seen that plentiful round pits and white block MC phases are distributed on the dimples; the round pits are formed by the desquamation of round hard particles. In addition, some tearing arris can be observed in Fig. 12. This kind of mixed fracture mechanism often occurs to the materials with the high strength and fine ductility. Commonly, large quantities of micro-holes accumulate at the front edge of

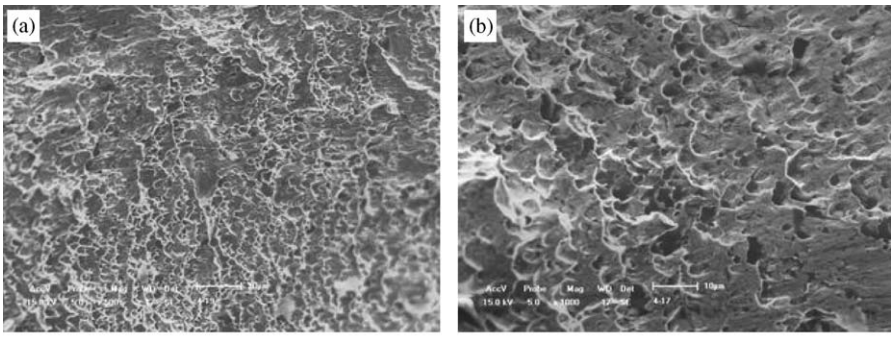

Fig. 12. SEM morphology of tensile fracture surface of LMDS-formed sample.

the main crack, and then the tearing arris link these areas, resulting in the rupture of the part.

Consequently, it can be confirmed that the fracture characteristic of LMDS-formed nickel-based superalloy samples, which is identical to that of the conventionally formed ones, is the ductile fracture behavior.

3.5. The microhardness of LMDS-fabricated parts

The microhardness is an important index to evaluate the material properties. It depends on both the composition and the microstructure. Fig. 13 exhibits the microhardness distribution of the longitudinal section of LMDS-formed thin-wall sample in the Z-direction, which is manufactured with the processing parameters given in Table 3. Horizontal ordinate represents the vertical distance from the substrate surface to the measuring point of the thin-wall sample; vertical ordinate represents the Vickers hardness of the measuring point. It can be concluded that the hardness at the bottom and top of the thin-wall sample is higher than the hardness at the middle of the thin-wall sample.

This phenomenon can be explained as follows. The hardness at the top of the thin-wall sample is higher owing to the refining microstructure of the cladding layers caused by the rapid melt and solidification of the material. However, the reason why the hardness at the middle of the thin-wall sample goes down can be clarified in detail. During the every cladding cycle, namely a reciprocating motion of the laser beam, the temperature in all positions of the prior-formed thin-wall sample goes through a cycle process in which the temperature changes from low to high, then to low again. Therefore, the prior-formed positions undergo multiple heat cycles. This effect is equivalent to the disposal of multiple tempers and aging. The earlier the position is formed, the more times it undergoes the heat cycle. Consequently, the hardness of prior-formed positions, especially the middle of the thin-wall sample, decreases because of this effect. But the hardness of the bottom of the thin-wall part goes up again, the reason is that the initial several cladding layers suffer from the forced cooling function of the substrate, so the temperature gradient in this region becomes evident, forming especially the close dendrites. In summary, the factors mentioned above cause the difference in the microhardness of different positions of the LMDS-formed thin-wall sample.

3.6. The microsegregation of LMDS-fabricated parts

Fig. 14 shows the distribution of main chemical elements of LMDS-formed thin-wall sample, whose processing parameters are given in Table 3, in the Z-direction. Horizontal ordinate represents the vertical distance from the substrate surface to the measuring point of the thin-wall sample; vertical ordinate represents the percents of several main chemical elements of thin-wall sample. It can be seen that the distribution of chemical elements is uniform, and there is hardly any composition segregation. Besides, the main chemical elements of the thin-wall sample approximately accord with those of alloy powder, so the LMDS technology can avoid the disadvantageous influences caused by the composition segregation in the process of conventional manufacturing technology, thereby improving the properties of the LMDS-formed parts.

The dendritic segregation results from the non-equilibrium solidification, and the degree of segregation is greatly affected by the extent of non-equilibrium solidification. The remarkable improvement of elemental segregation of LMDS-formed parts relates to two factors: Firstly, under the condition of the excessively high temperature gradient and rapid solidification rate, the solidification process departures from the equilibrium state obviously. Accordingly, the solute catch effect enhances so that the solute partition coefficient drives to 1, so the composition of solidification phases tends to the average composition of

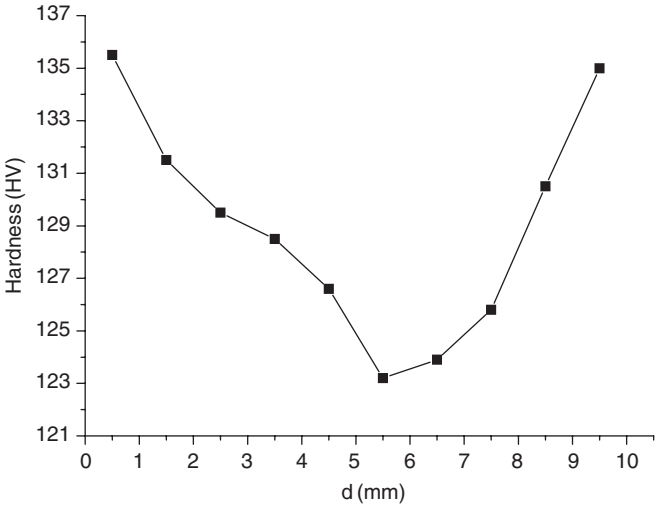

Fig. 13. Hardness distribution in the Z-direction of LMDS-formed thin-wall sample.

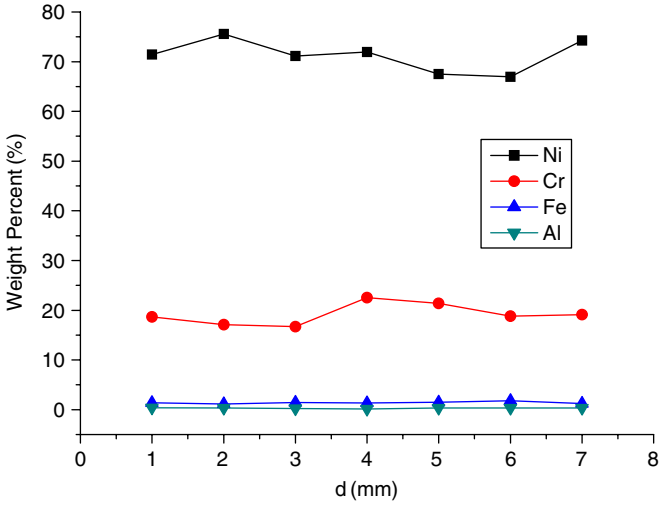

Fig. 14. Composition distribution in the Z-direction of LMDS-formed thin-wall sample.

alloy powder. Secondly, the exceeding refining of microstructure leads to the uniformity effect of alloy elements, which is induced by the elemental diffusion in the solid phases, enhances. Furthermore, the decrease, dispersion and thinning of the interdendritic-precipitated phases all benefit the uniform distribution of the alloy elements.

4. Conclusion

Based on the LMDS system, comprehensive experiments are carried out with nickel-based superalloy to systematically investigate the influences of the processing parameters on forming characteristics. The following conclusions can be drawn up:

(1) Both the height of single-cladding layer and the width of single cladding pass are the most important characteristics of LMDS-fabricated components and they are regularly affected by almost all of the processing parameters, especially the laser power, spot diameter, scanning velocity and powder-feeding rate.
(2) The smoothness of forming surface is another particularly significant forming characteristic of the LMDS process. Choosing the appropriate scanning space is the key to obtain smooth scanning plane, which builds up to form the parts.
(3) Through the systematic experiments, a series of optimal processing parameters can be acquired by observing the forming characteristics. According to the optimal parameters, some nickel-based superalloy parts with near-net shape and full density are fabricated with flying colors.
(4) The solidification microstructure of cladding layer is composed of parallel dendrites whose growing direction is from bottom to top and vertical to the substrate, and the dendrites take on the look of typical directional solidification microstructure in the altitude direction. By contrast, minute equiaxed grains appear on the top of the fine dendrites.
(5) The LMDS-formed parts hold fine mechanical properties, and SEM morphology of tensile fracture surface indicates the LMDS-formed parts possess rather high ductility.
(6) The distribution of chemical composition of LMDS-formed parts is uniform, and there is hardly any composition segregation, so the LMDS technology can avoid the disadvantageous influences caused by the composition segregation in the process of conventional manufacturing technology, thereby improving the properties of the LMDS-formed parts.

Acknowledgements

Financial support from National "863" High-technology Research Project (under the contract no. 2002AA420060) is greatly appreciated.

References

[1] Pham DT, Gault RS. A comparison of rapid prototyping technologies. Int J Mach Tools Manuf 1998;38(10–11):1257–87.
[2] Kobryn PA, Moore EH, Semiatin SL. The effect of laser power and traverse speed on microstructure, porosity, and build height in laser deposited Ti–6Al–4V. Scr Mater 2000;43(4):299–305.
[3] Griffith ML, Schlienger ME, Harwell LD, et al. Understanding thermal behavior in the LENS process. Mater Des 1999;20(2–3):107–13.
[4] Hu D, Kovacevic R. Sensing, modeling and control for laser-based additive manufacturing. Int J Mach Tools Manuf 2003;43(1):51–60.
[5] Choi J, Chang Y. Characteristics of laser aided direct metal/material deposition process for tool steel. Int J Mach Tools Manuf 2005;45(4–5):597–607.
[6] Peng L, Taiping Y, Sheng L, Dongsheng L, Qianwu H, Weihao X, et al. Direct laser fabrication of nickel alloy samples. Int J Mach Tools Manuf 2005;45(11):1288–94.
[7] Jeng JY, Peng SC, Chou CJ. Metal rapid prototype fabrication using selective laser cladding technology. Int J Adv Manuf Technol 2000;16(9):681–7.
[8] Zhang Y, Xi M, Gao S, Shi L. Characterization of laser direct deposited metallic parts. J Mater Process Technol 2003;142(2):582–5.
[9] Li Y, Yang H, Lin X, Huang W, Li J, Zhou Y. The influences of processing parameters on forming characterizations during laser rapid forming. Mater Sci Eng A 2003;360(1–2):18–25.
[10] Ning G, Zhong M, Yang L, Liu W, Chen Y, Li F. Research about close-loop control system during laser direct manufacturing metallic components. Appl Laser 2002;22(2):172–6.
[11] Li Y. Research on technical characters and microstructure of laser solid forming. Ph.D. dissertation, Northwestern Polytechnical University, 2001.